

## Electronic structure of strained InP/Ga<sub>0.51</sub>In<sub>0.49</sub>P quantum dots

Craig Pryor,\* M-E. Pistol, and L. Samuelson

Department of Solid State Physics, Box 118, Lund University, S-221 00 Lund, Sweden

(Received 14 March 1997)

We calculate the electronic structure of nm scale InP islands embedded in Ga<sub>0.51</sub>In<sub>0.49</sub>P. The calculations are done in the envelope approximation and include the effects of strain, piezoelectric polarization, and mixing among 6 valence bands. The electrons are confined within the entire island, while the holes are confined to strain induced pockets. One pocket forms a ring at the bottom of the island near the substrate interface, while the other is above the island in the GaInP. The two sets of hole states are decoupled. Polarization dependent dipole matrix elements are calculated for both types of hole states. [S0163-1829(97)06039-6]

### I. INTRODUCTION

In recent years great progress has been made in the fabrication and measurement of semiconductor quantum dots made by Stranski-Krastonov growth. In this technique, material is deposited epitaxially onto a substrate that is lattice mismatched to the deposited material. Due to the mismatch, the deposited material spontaneously forms nanometer scale islands, the size and shape of which are both material and growth-condition dependent. The pyramidal shape and presence of strain in the islands makes for a potentially rich electronic structure. Theoretical studies of strained islands have employed various degrees of approximation to the geometry, strain distribution, and electron dynamics, ranging from single band models of hydrostatically strained islands, to multiband models including realistic shapes and strain distributions.<sup>1-4</sup>

In this paper we consider InP islands buried in Ga<sub>0.51</sub>In<sub>0.49</sub>P,<sup>5</sup> a material combination that has so far received little theoretical attention. The geometry is made as realistic as possible by adopting the shape shown in Fig. 1, which has been observed using atomic force microscopy and transmission electron microscopy.<sup>5</sup> We assume that different size islands have the same shape as shown in Fig. 1, but are simply rescaled. We parametrize the size of the island by the height in the  $\hat{z}$  direction,  $h$ . In most of the calculations we use  $h = 15$  nm, but we will consider variations as well. Note that the wetting layer is not included in our calculation. The wetting layer does not significantly alter the strain distribution in the island because it is pseudomorphically strained. Also, its measured thickness is on the order of the grid spacing used, and hence its inclusion in the electronic structure portion of the calculation would be unjustified. The calculation is done in two steps: the strain distribution is determined using continuum elastic theory, and then used in a strain-dependent  $\mathbf{k}\cdot\mathbf{p}$  Hamiltonian.

### II. STRAIN

The strain is computed by minimizing the free energy for a cubic crystal,<sup>6</sup>

$$F = \int d^3x \left[ \frac{1}{2} C_{xxxx} (\sigma_{xx}^2 + \sigma_{yy}^2 + \sigma_{zz}^2) + C_{xxyy} (\sigma_{xx}\sigma_{yy} + \sigma_{xx}\sigma_{zz} + \sigma_{yy}\sigma_{zz}) + 2C_{xyxy} (\sigma_{xy}^2 + \sigma_{xz}^2 + \sigma_{yz}^2) - \alpha (\sigma_{xx} + \sigma_{yy} + \sigma_{zz}) \right], \quad (2.1)$$

where  $\sigma_{ij}$  is the strain tensor, the  $C$ 's are material dependent elastic constants, and  $\alpha$  is a parameter used to enforce the lattice mismatch between the two materials. The strain is given in terms of the displacement by  $\sigma_{ij} = \frac{1}{2} (\partial_i u_j + \partial_j u_i)$ .  $F$  is constructed as a function of the  $u_i$ 's on a cubic grid with derivatives replaced by differences, and then  $F$  is minimized using the conjugate gradient algorithm. The grid consisted of a periodic box of  $130 \times 130 \times 120$  sites with the island contained within a  $65 \times 65 \times 20$  region. The grid is reduced 1/4 by exploiting the symmetries of the system. The size of the box is chosen sufficiently large to make the band energies within 1% of the bulk Ga<sub>0.51</sub>In<sub>0.49</sub>P values at the points furthest from the island. Errors due to the finite system should be  $\leq 1\%$  at the island. No constraints need to be directly imposed on the minimization since far from the island the strain has relaxed to its bulk ( $=0$ ) value.

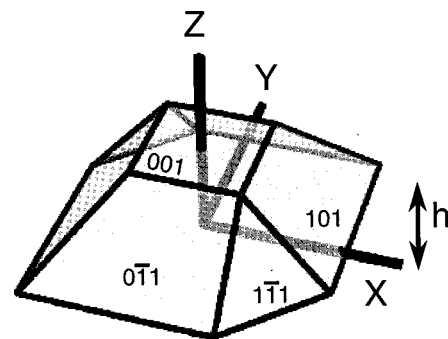


FIG. 1. Island geometry. The distances to the  $\{011\}$  and  $\{\bar{1}11\}$  planes measured from the center of the base of the island are in the ratio  $d_{011}/d_{\bar{1}11} \approx 1$ .

The lattice mismatch between the two materials is implemented as follows. The grid is chosen to be commensurate with the barrier material so the grid corresponds to some multiple of the barrier material's *crystal* unit cell. Then for unstrained barrier material we would have  $u_i=0$ . But this means that the grid is wrong for the island material since it has a different crystal unit cell. Unstrained island material should actually have a nonzero  $u_i$  to reflect the fact that its crystal unit cell has a different size. If the island and barrier lattice constants are  $a_I$  and  $a_B$ , respectively, then setting  $\alpha=(C_{xxx}+2C_{xyy})(a_I-a_B)/a_B$  in the island causes the minimum of  $F$  to be at  $\sigma_{ij}^0=\delta_{ij}(a_I-a_B)/a_B$ , which is the desired amount of strain in the grid. Because  $\sigma_{ij}^0$  is completely fictitious, and reflects only the straining of the coordinate system, the physical strain is obtained by subtracting  $\sigma_{ij}^0$  from the  $\sigma_{ij}$  which minimizes  $F$  for the heterostructure.

There is some freedom in the choice of grid differences used to approximate  $F$ . Using symmetric differences,  $\partial_x f(x) \rightarrow [f(x+h)-f(x-h)]/2h$ , produces oscillatory solutions that must be smoothed. Oscillatory solutions are in fact a common problem with finite difference approximations to equations involving first derivatives. For the case at hand this problem is avoided by evaluating  $F$  within each unit cube as a function of the  $u_i$ 's at the eight corners. This is essentially a low-order finite element method. Although more sophisticated approximations may yield more accurate strains, we are constrained by the fact that the strain is to be used with the cubic grid, which is most convenient for the electronic structure part of the calculation. Only one strain field is needed for all sizes since it is a dimensionless quantity, and the strain for a different island size is obtained by a trivial rescaling.

Because the materials lack inversion symmetry the strain produces a polarization given by  $P_i=e_{ijk}\sigma_{jk}$ , leading to an additional electrostatic potential. For III-IV semiconductors, the only nonzero elements of the piezoelectric tensor are  $e_{xyz}=e_{zxy}=e_{yzx}\equiv e_{14}$ . From the polarization it is a simple matter to compute the electrostatic potential  $V_p$  by numerically solving Poisson's equation. Dipoles are induced at some of the edges, and on the  $\{1\bar{1}\bar{1}\}$  and  $\{\bar{1}11\}$  faces. Because the islands are primarily under compression the faces have a negative charge (Fig. 2). The piezoelectric effect contributes only a small amount to the potential felt by carriers in the island, and most of the modification of the potential is outside the island, as seen in Fig. 2. In studies of InAs islands the piezoelectric potential was important because the islands were assumed to have fourfold rotational symmetry that was broken by the piezoelectric potential.<sup>2</sup> The six-sided InP islands lack such a symmetry to begin with, and the piezoelectric potential does not make a qualitative change in the spectrum.

### III. HAMILTONIAN

The electronic structure is calculated in the envelope approximation using  $\sigma_{ij}$  and  $V_p$  computed above. The electron Hamiltonian is<sup>7</sup>

$$H_e = E_c - \frac{\hbar^2}{2m} \nabla^2 + a_c \sigma - eV_p, \quad (3.1)$$

where  $E_c$  is the local conduction-band edge in the absence of strain,  $a_c$  is the conduction-band deformation potential, and  $\sigma = \text{tr} \sigma_{ij}$ . For the valence band we used a 6-band model given by<sup>7</sup>

$$H_h = H_0 + H_s - eV_p, \quad (3.2)$$

$$H_0 = \begin{pmatrix} -P+Q & -S^* & R & 0 & \sqrt{\frac{3}{2}}S & -\sqrt{2}Q \\ -S & -P-Q & 0 & R & -\sqrt{2}R & \frac{1}{\sqrt{2}}S \\ R^* & 0 & -P-Q & S^* & \frac{1}{\sqrt{2}}S^* & \sqrt{2}R^* \\ 0 & R^* & S & -P+Q & \sqrt{2}Q & \sqrt{\frac{3}{2}}S^* \\ \sqrt{\frac{3}{2}}S^* & -\sqrt{2}R^* & \frac{1}{\sqrt{2}}S & \sqrt{2}Q & -P-\Delta & 0 \\ -\sqrt{2}Q & \frac{1}{\sqrt{2}}S^* & \sqrt{2}R & \sqrt{\frac{3}{2}}S & 0 & -P-\Delta \end{pmatrix}, \quad (3.3)$$

$$P = -E_v - \gamma_1 \frac{\hbar^2}{2m_0} (\partial_x^2 + \partial_y^2 + \partial_z^2), \quad (3.4)$$

$$Q = -\gamma_2 \frac{\hbar^2}{2m_0} (\partial_x^2 + \partial_y^2 - 2\partial_z^2), \quad (3.5)$$

$$R = \sqrt{3} \frac{\hbar^2}{2m_0} [\gamma_2(\partial_x^2 - \partial_y^2) - 2i\gamma_3\partial_x\partial_y], \quad (3.6)$$

$$S = -\sqrt{3}\gamma_3 \frac{\hbar^2}{m_0} \partial_z(\partial_x - i\partial_y), \quad (3.7)$$

where  $E_v$  is the unstrained local valence-band edge, and  $\gamma_i$  are the Luttinger parameters. Since the Luttinger parameters vary spatially, we used the prescription  $\gamma_i \partial_x^2 \rightarrow \partial_x \gamma_i \partial_x$ .

The strain-dependent coupling is given by<sup>7</sup>

$$H_s = \begin{pmatrix} -p+q & -s^* & r & 0 & \sqrt{\frac{3}{2}}s & -\sqrt{2}q \\ -s & -p-q & 0 & r & -\sqrt{2}r & \frac{1}{\sqrt{2}}s \\ r^* & 0 & -p-q & s^* & \frac{1}{\sqrt{2}}s^* & \sqrt{2}r^* \\ 0 & r^* & s & -p+q & \sqrt{2}q & \sqrt{\frac{3}{2}}s^* \\ \sqrt{\frac{3}{2}}s^* & -\sqrt{2}r^* & \frac{1}{\sqrt{2}}s & \sqrt{2}q & -a_v e & 0 \\ -\sqrt{2}q & \frac{1}{\sqrt{2}}s^* & \sqrt{2}r & \sqrt{\frac{3}{2}}s & 0 & -a_v e \end{pmatrix}, \quad (3.8)$$

$$p = a(\sigma_{xx} + \sigma_{yy} + \sigma_{zz}), \quad (3.9)$$

$$q = b[\sigma_{zz} - \frac{1}{2}(\sigma_{xx} + \sigma_{yy})], \quad (3.10)$$

$$r = \frac{\sqrt{3}}{2}b(\sigma_{xx} - \sigma_{yy}) - id\sigma_{xy}, \quad (3.11)$$

$$s = -d(\sigma_{xz} - i\sigma_{yz}), \quad (3.12)$$

where  $a_v$ ,  $b$ , and  $c$  are the hydrostatic and two shear deformation potentials. The four-band model may be obtained by taking  $\Delta \rightarrow \infty$ .

#### IV. MATERIAL PARAMETERS

The values used for the various material parameters are given in Table I. These vary considerably in the accuracy with which they have been measured, with the deformation potentials suffering the most uncertainty. There is a paucity of data on  $\text{Ga}_{0.51}\text{In}_{0.49}\text{P}$ , and most quantities are determined by interpolating between InP and GaP. The conduction-band effective mass in  $\text{Ga}_{0.51}\text{In}_{0.49}\text{P}$  is simply set to the value for InP, since interpolation is complicated by the fact that GaP is indirect. The hydrostatic deformation potentials for  $\text{Ga}_{0.51}\text{In}_{0.49}\text{P}$ ,  $a_c$  and  $a_v$ , are estimated by assuming  $a_c/a_v$  is the same as for InP, while  $a_g = a_v + a_c$  is taken from  $\text{Ga}_{0.51}\text{In}_{0.49}\text{P}$  measurements.<sup>8,9</sup> In computing  $V_p$ , the dielectric constant is assumed to take on the InP value throughout the system.

One parameter that bears special mention is the unstrained valence-band offset (i.e., the InP valence-band energy referenced to that of the  $\text{Ga}_{0.51}\text{In}_{0.49}\text{P}$ , in the absence of strain). The value used is based on transition-metal impurity spectra, and is in agreement with the value based on Au Schottky barrier data.<sup>10</sup> The idea is that transition-metal impurities are empirically observed to have energy levels fixed with respect to the vacuum, relatively independent of their host environment. Thus, by comparing band edges referenced to the impurity levels in two different materials one deduces the relative band offsets if the strain could be turned off. The ground-state energies of Fe impurities are 0.785 and 0.74 eV above the valence band in InP and  $\text{Ga}_{0.51}\text{In}_{0.49}\text{P}$ , respectively,<sup>11</sup> so the InP valence band is 45 meV below  $\text{Ga}_{0.51}\text{In}_{0.49}\text{P}$ .

#### V. ELECTRONIC STRUCTURE

Before solving Schrödinger's equation it is instructive to examine the band structure shown in Fig. 3. The conduction band is rather ordinary, with electrons confined to the island

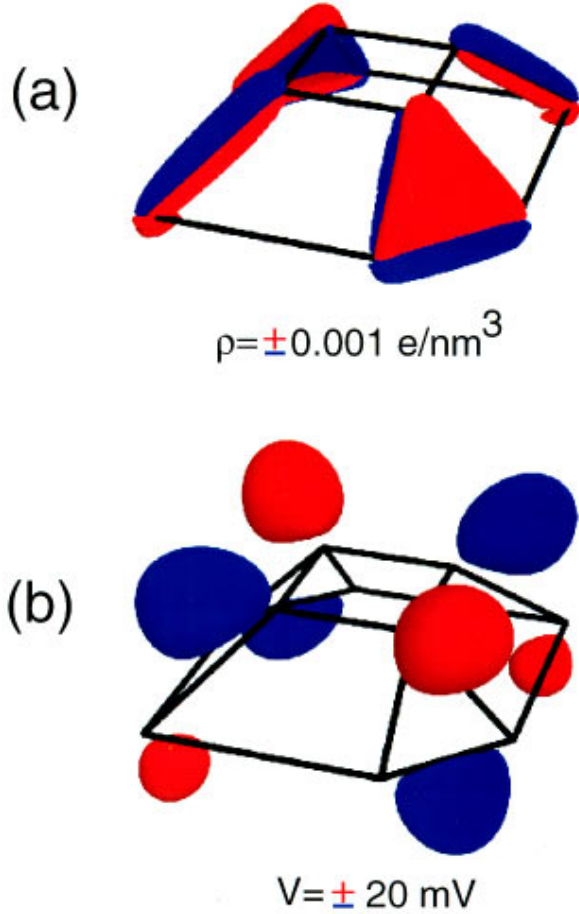


FIG. 2. (Color) Piezoelectric effect for an island with  $h = 15 \text{ nm}$ . (a) Piezoelectric charge density. The red surface is the contour of  $\rho = +0.001 e/\text{nm}^3$ , blue surface indicates  $\rho = -0.001 e/\text{nm}^3$ . (b) Electrostatic potential due to the piezoelectric polarization  $V_p$ . The red surface is the contour of  $V_p = +20 \text{ mV}$ , blue surface indicates  $V_p = -20 \text{ mV}$ .

by a barrier of about 250 meV at the InP/Ga<sub>0.51</sub>In<sub>0.49</sub>P interface. Strain reduces the barrier height, but since most of the band offset resides in the conduction band, there is still a substantial barrier. There is also some modification of the band edge inside the island, but for the most part it looks like a particle in a box. The barrier height of 250 meV is in good agreement with measurements using deep-level transient spectroscopy, which give a barrier height of 240 meV.<sup>12</sup>

The valence band has a very complex structure. Note that in the absence of strain the island would actually be a weak antidot since the InP unstrained valence-band offset is  $-45 \text{ meV}$ ; the hole confinement is due entirely to strain. The valence-band edge has peaks near the bottom corners of the island which extend around the base in a ring. The highest points in this ring lie near the  $\{111\}$  planes. Because of the shallowness of the hole potential, the piezoelectric potential has a greater impact on the holes than on the electrons. Looking along the  $\hat{z}$  axis we see the valence band also has peaks in the Ga<sub>0.51</sub>In<sub>0.49</sub>P immediately above and below the island.

The confined state energies and wave functions are found by diagonalization of a finite difference version of the Hamiltonian using the Lanczos algorithm. This is done on

TABLE I. Material parameters. Unless otherwise noted, InP values are taken from Ref. 11, and Ga<sub>0.51</sub>In<sub>0.49</sub>P values are interpolated between InP and GaP values from Ref. 11.

Parameter	InP	Ga <sub>0.51</sub> In <sub>0.49</sub> P
$m_c$	$0.077m_0$	$0.077m_0^a$
$\gamma_1$	4.95	5.24
$\gamma_2$	1.65	1.53
$\gamma_3$	2.35	2.21
$E_g$	1.424 eV	1.97 eV <sup>b</sup>
$\Delta$	0.11 eV	0.095 eV
$a_{\text{gap}}$	$-6.6 \text{ eV}$	$-7.1 \text{ eV}^b$
$a_c$	$-7.0 \text{ eV}^c$	$-7.5 \text{ eV}^d$
$a_v$	0.4 eV	0.4 eV <sup>d</sup>
$b$	$-2.0 \text{ eV}$	$-1.9 \text{ eV}$
$d$	$-5.0 \text{ eV}$	$-4.75 \text{ eV}$
$e_{14}$	$0.035 \text{ C/m}^2^e$	$0.068 \text{ C/m}^2^e$
$\epsilon_R$	12.61	12.61 <sup>a</sup>
$C_{xxxx}$	$10.22 \times 10^{11} \text{ dyn/cm}^2$	$12.17 \times 10^{11} \text{ dyn/cm}^2$
$C_{xyxy}$	$5.76 \times 10^{11} \text{ dyn/cm}^2$	$6.01 \times 10^{11} \text{ dyn/cm}^2$
$C_{xyxy}$	$4.6 \times 10^{11} \text{ dyn/cm}^2$	$5.82 \times 10^{11} \text{ dyn/cm}^2$
$a$	0.58687 nm	0.56532 nm

<sup>a</sup>Value for InP used.

<sup>b</sup>Reference 9.

<sup>c</sup>Reference 8.

<sup>d</sup>See text.

<sup>e</sup>Reference 14.

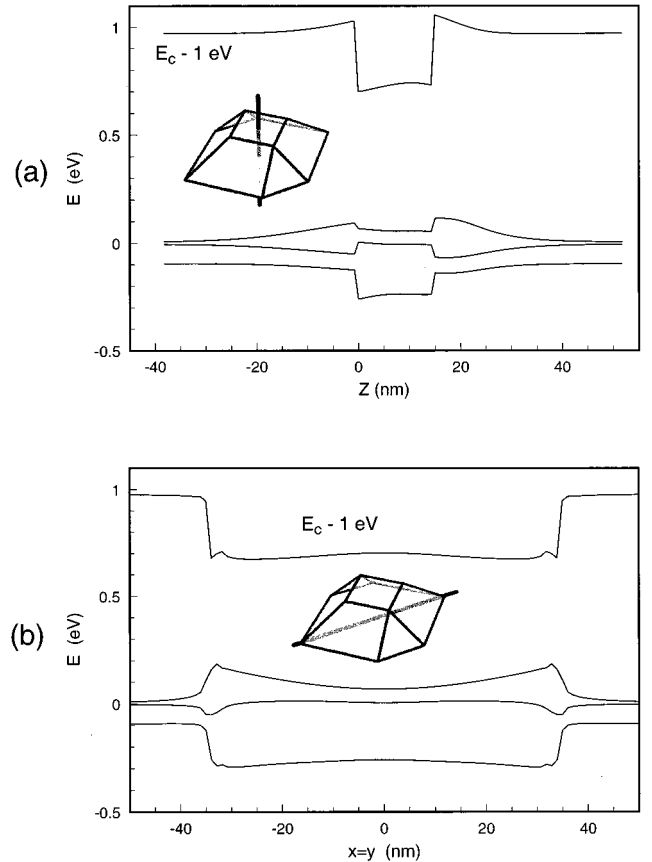


FIG. 3. Band diagrams with inclusion of strain. Scale shown is for  $h = 15 \text{ nm}$ , but other island sizes are obtained by simply rescaling. (a) Along the  $\hat{z}$  direction, through the center of the island. (b) Along the line  $x = y$  passing through the base of the island.

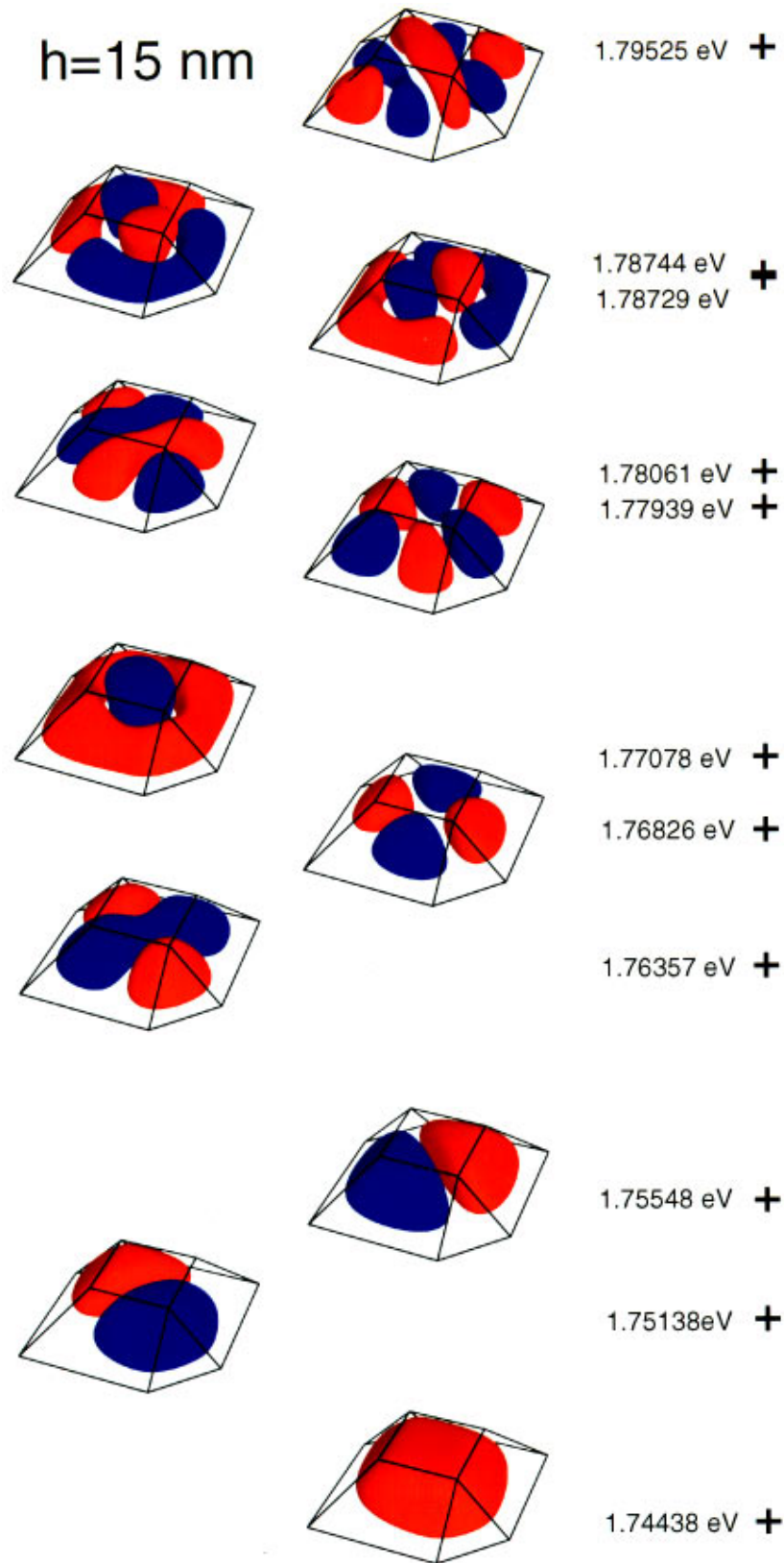


FIG. 4. (Color) Conduction-band wave functions and corresponding energies for  $h=15$  nm. Red (blue) indicates positive (negative)  $\psi$ .

the same cubic grid used to compute the strain, the only difference being that it is truncated to exclude unnecessary regions of barrier material. The symmetry of the island is not used to reduce the grid.

The first few conduction-band wave functions are shown

in Fig. 4. These states are relatively simple to understand if one crudely approximates the truncated pyramid as a flat box that is smallest in the  $\hat{z}$  direction. The low-lying states all correspond to excitations in the  $\hat{x}$  and  $\hat{y}$  directions. One manifestation of the strain is the ordering of the first and

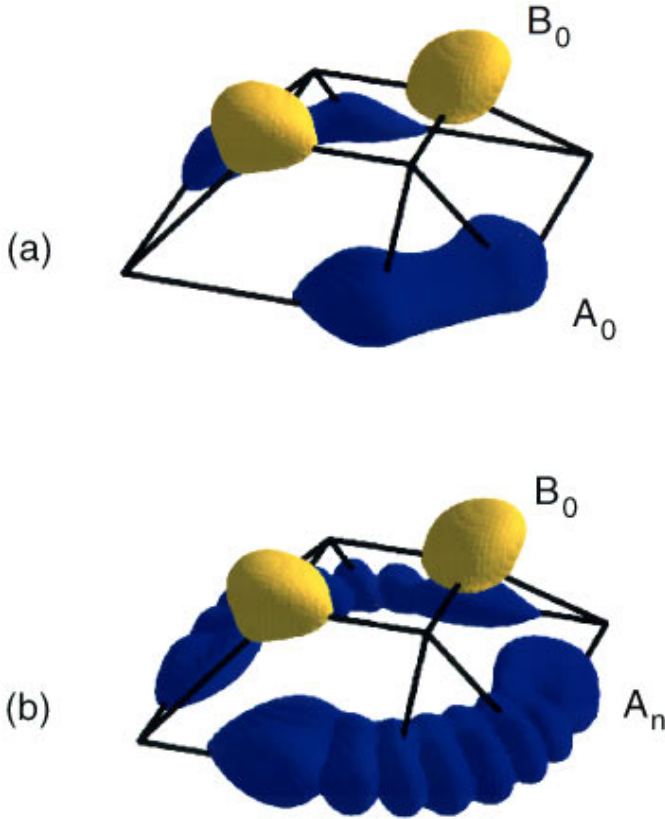


FIG. 5. (Color) Valence-band wave functions for  $h = 15$  nm. The contours are of  $\sum_i |\psi_i|^2$  equal to 0.01 of the peak value. (a) Blue surface is the ground state,  $A_0$ , yellow surface is the highest state located above the island,  $B_0$ . (b) Blue surface is the excited state  $A_n$  immediately above  $B_0$  in energy.

second excited states, which appears reversed from the naive expectation. If the island were a simple box, the state with a node along the  $[1\bar{1}0]$  direction would be higher since the island is shorter in that direction. However, strain modifies the potential, resulting in a different ordering of states.

The valence-band states have a more complex structure, as seen in Fig. 5. The states fall into two categories: states localized near the bottom of the island, labeled  $A_n$ , and those localized above the island in the  $\text{Ga}_{0.51}\text{In}_{0.49}\text{P}$ , labeled  $B_n$ . The ground state is  $A_0$ , which is peaked around the band-edge maxima near the  $\{111\}$  planes. Excited states (lower valence band energy) extend around the ring at the base of the island. The first type  $B$  state,  $B_0$ , appears 15 meV from the ground state. Although the band diagram shows a pocket below the island, there are no localized states there. The localized valence-band states provide a partial explanation for the observation of multiple lines seen in photoluminescence (PL).<sup>13</sup> An excited hole that relaxed into a  $B$  state would be unable to transfer into one of the  $A$  states, and would instead recombine with an electron in its ground state. Examination of the valence-band wave functions shows that including the split-off band is not a superfluous addition. The split-off component is typically of order 0.2 of the largest component.

Since island size depends on growth conditions it is inter-

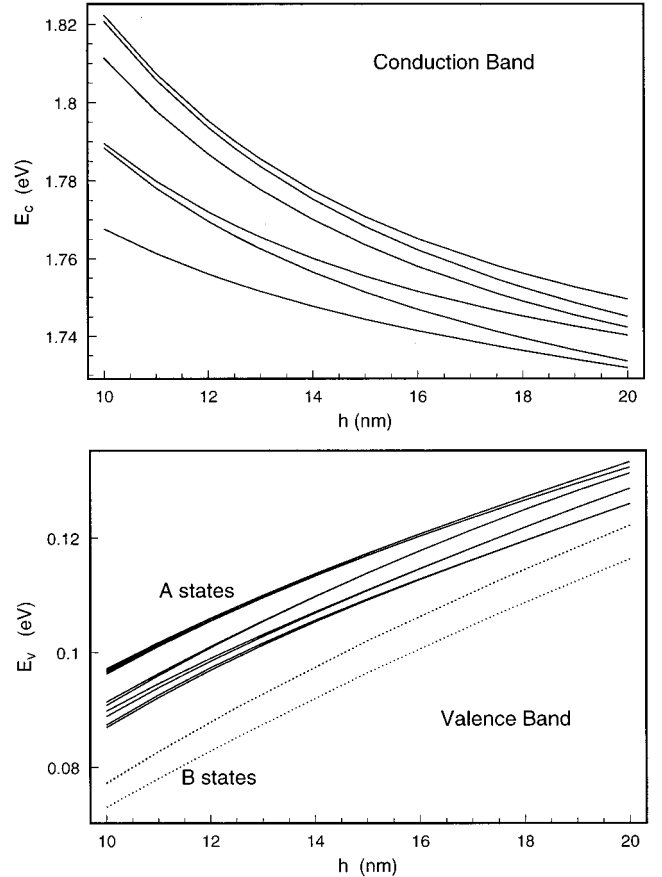


FIG. 6. Energies as a function of island size. (a) Electron states. (b) Valence band. Only the first few  $A$  states are shown, so there are missing states between the lowest  $A$  state and the highest  $B$  state ( $B_0$ ).

esting to examine the dependence of energy on island size, as shown in Fig. 6. The conduction-band spacings are of order 10 meV for a height of 15 nm, increasing to 20 meV for a 10 nm island. The hole spacings are much smaller due to their higher effective mass, and the dependence on  $h$  is more complex due to the odd-shaped potential. It should be noted that although the spacings are not monotonic in  $h$ , the individual energies are.

## VI. TRANSITIONS

Knowledge of transition rates are important for determining which states will be experimentally accessible. In order for the  $B$  states to produce an observable PL line the  $B \rightarrow A$  transition rate must be sufficiently slow that recombination occurs before relaxation into an  $A$  state. A simple method of analysis is to compare the relaxation rates for  $B_0 \rightarrow A_n$  with  $A_n \rightarrow A_{n-1}$ , where  $A_n$  is the  $A$  state closest in energy into which the  $B_0$  state could relax. If, for example, we assume the transition is due to emission of an acoustic phonon, the rate is given by  $T_{i \rightarrow f} \propto \langle |f| \exp(i\mathbf{q} \cdot \mathbf{r}) |i\rangle|^2$ . The calculated wave functions give  $T_{B_0 \rightarrow A_n} \lesssim 10^{-12} T_{A_n \rightarrow A_{n-1}}$  for  $\mathbf{q}$  throughout the Brillouin zone. This suppression is due entirely to the

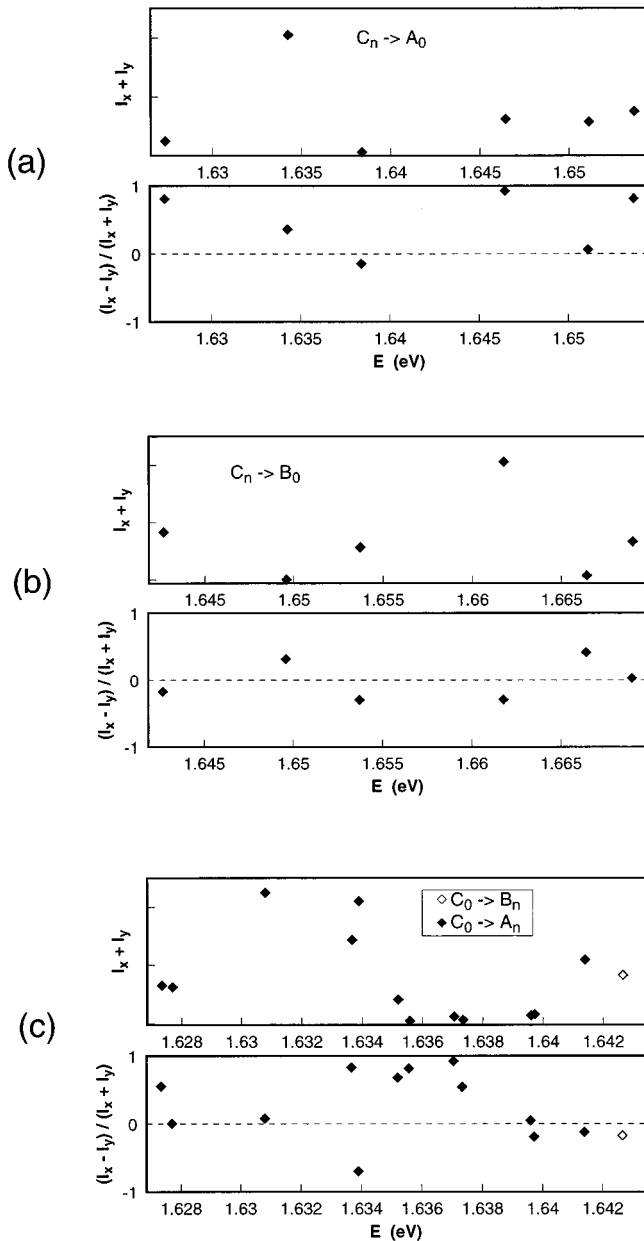


FIG. 7. Magnitude and polarization dependence of band-to-band optical matrix elements for an island with  $h=15$  nm.  $I_x + I_y$  is in equal arbitrary units in all three figures. (a) Transitions from first six conduction-band states  $C_n$  to valence-band state  $A_0$ . (b) Transitions from first six conduction-band states  $C_n$  to valence-band state  $B_0$ . (c) Transitions from conduction-band ground state  $C_0$  to valence-band states  $A_0, \dots, A_{14}, B_0$ . Transitions spaced less than 0.1 meV apart have been combined.

highly localized nature of the states, so a comparable suppression will be obtained for other relaxation processes.

Since multiple PL lines are observed experimentally, it behooves us to examine optical transitions involving excited states. The strength and polarization dependence of the ra-

diative transitions are found by computing the dipole matrix elements. These are computed by decomposing the envelope wave functions into linear combinations of the states  $\langle X|$ ,  $\langle Y|$ ,  $\langle Z|$ , and  $\langle S|$ , and using the fact that only  $\langle X|p_x|S\rangle = \langle Y|p_y|S\rangle = \langle Z|p_z|S\rangle$  is nonzero. The matrix elements are calculated for light in the  $\hat{z}$  direction for both possible polarizations. The results are shown in Fig. 7, where  $I_x$  and  $I_y$  are the squares of the dipole matrix elements for light polarized in the  $\hat{x}$  and  $\hat{y}$  directions, respectively. Casual examination of the wave functions might lead one to believe that the transition involving the  $B$  state would be suppressed since it is type II. This concern is seen to be unfounded, and the transition rate from the  $B$  state is comparable to that from the  $A$  state. The  $B$  transitions are highly suppressed for conduction-band states that are antisymmetric about the  $[110]$  direction. The  $A$  transitions are less selective, but still show strong polarization dependence. The most notable feature of transitions between the conduction-band ground state and the valence-band states  $A_n$  is that they are predominantly polarized in the  $\hat{x}$  direction. Therefore, even if there is mixing of the  $A$  states, the resulting transition should still be polarized in the  $\hat{x}$  direction.

## VII. CONCLUSIONS

Comparison with PL measurements shows good agreement with the major features.<sup>13</sup> PL of single quantum dots shows energies in the range 1.62–1.64 eV, which corresponds to the calculated energies for island heights in the range 14–17 nm. The calculated PL spacing of 15 meV for  $h=15$  nm is in agreement with the observed multiple PL lines, which are 10–20 meV apart. Experiments on single islands show as many as four lines, which the current model is unable to explain. It should be noted, however, that macroscopic PL measurements that necessarily average over a range of island sizes and shapes, typically show two peaks spaced 15–20 meV apart. Therefore the dominant characteristic of the spectrum is consistent with the valence-band double-well potential. The additional lines appear to be due to some further structure. The extra structure could be due to asymmetry of the islands, which would each split each of the  $A$  and  $B$  states into two localized states, giving a total of four lines. While appealing, this model is difficult to reconcile with the observation that the islands have a high degree of symmetry.<sup>5</sup>

In summary, we have shown that InP islands have a rich electronic structure, with holes confined to multiple pockets in and around the island. The energy levels are consistent with measurements on single dots, and the calculated structure can produce two PL lines 15 meV apart. While the predicted doubling of PL lines provides an important existence proof, more work is needed to fully explain the puzzling proliferation of lines seen in experiments.

\*Electronic address: cpryor@zariski.ftf.lth.se

<sup>1</sup>J.-Y. Marzin and G. Bastard, *Solid State Commun.* **91**, 39 (1994).

<sup>2</sup>M. Grundmann, O. Stier, and D. Bimberg, *Phys. Rev. B* **52**, 11 969 (1995).

<sup>3</sup>M. A. Cusack, P. R. Briddon, and M. Jaros, *Phys. Rev. B* **54**, 2300 (1996).

<sup>4</sup>H. Fu and A. Zunger *Phys. Rev. B* **55**, 1642 (1997), and references therein.

- <sup>5</sup>K. Georgsson *et al.*, Appl. Phys. Lett. **67**, 2981 (1995).
- <sup>6</sup>L. D. Landau and E. M. Lifshitz, *Theory of Elasticity* (Pergamon, London, 1959).
- <sup>7</sup>T. B. Bahder, Phys. Rev. B **45**, 1629 (1992); *ibid.* **41**, 11 992 (1990).
- <sup>8</sup>D. D. Nolte, W. Walukiewicz, and E. E. Haller, Phys. Rev. Lett. **59**, 501 (1987).
- <sup>9</sup>S. W. Tozer, D. J. Woford, J. A. Bradley, and D. Bour, in *19th International Conference of the Physics of Semiconductors*, edited by W. Zawadski (Polish Academy of Sciences, 1988), Vol. 2, p. 881.
- <sup>10</sup>S. Tiwari and D. J. Frank, Appl. Phys. Lett. **60**, 630 (1992).
- <sup>11</sup>*Semiconductors*, edited by O. Madelung, M. Schilz, and H. Weiss, Landolt-Börnstein, New Series, Vol. 17 (Springer-Verlag, New York, 1982).
- <sup>12</sup>S. Anaud, N. Carlsson, M.-E. Pistol, L. Samuelson, and W. Seifert, Appl. Phys. Lett. **67**, 3016 (1995).
- <sup>13</sup>D. Hessman, P. Castrillo, M.-E. Pistol, C. Pryor, and L. Samuelson, Appl. Phys. Lett. **69**, 749 (1996).
- <sup>14</sup>S. Adachi, J. Appl. Phys. **53**, 8775 (1982).